THE BELL SYSTEM TECHNICAL JOURNAL
Vol. 51, No. 9, November, 1972
Printed in U.S.A.

Stability Considerations in Nonlinear Feedback Structures as Applied to Active Networks

By M. BAUMWOLSPINER

(Manuscript received April 24, 1972)

Active filters have recently acquired widespread use in the realization of frequency-selective networks. Unlike their passive counterparts, active filters have the potential of oscillating.

Furthermore, it has been observed that the onset of oscillations in biquad active filters is dependent upon signal level. This led to the recognition that nonlinear stability theory would be necessary to comprehend this behavior.

This paper develops a technique to analyze the stability of networks containing linear and nonlinear elements interconnected in multifeedback structures. This is accomplished by extending the concept of the "Describing Function" to include networks containing nonlinearities with frequency-dependent linear feedback. The technique is then applied to explain qualitatively and quantitatively nonlinear effects in op-amps and their relation to the stability of frequency-selective networks containing them (e.g., the Multiple Amplifier Biquad, MAB, and the Single Amplifier Biquad, SAB). The technique is also applied to explain frequency shifts in amplitude-limited oscillators. The most valuable result of this analysis is the discovery of nonlinear feedback circuits which circumvent the conditional stability of high-frequency biquads. This has allowed us to obtain Q's of 50 at 100 kHz in a MAB employing 709 op amps. Similarly, a MAB employing 702 op amps was made to operate at 2 MHz with a Q of 10.

I. INTRODUCTION

In this paper, we shall deal primarily with a frequency-domain approach of analyzing networks containing linear and nonlinear elements interconnected as multifeedback structures. Particular applications will include the Single Amplifier Biquad[1] (SAB), the Multiple Amplifier Biquad[2] (MAB), and amplitude stabilized oscillators.

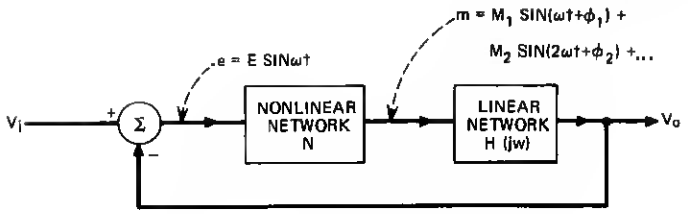

Fig. 1—A typical system with separable networks.

Our interest in this subject is motivated by conditional stability problems in biquads designed to operate above certain critical frequencies. Above these frequencies, these filters exhibit oscillatory modes when certain excitations are or were present. In the past, these conditional stability problems have been attributed to slew rate limiting in the operational amplifiers. However, we shall demonstrate later that although slew rate limiting may affect the stability, it is neither a necessary nor sufficient condition for conditional stability to occur in the MAB circuit.

We shall draw heavily on the Describing Function (DF) and the Dual Input Describing Function (DIDF) Techniques.[3-5] These techniques have the virtue of imparting a conceptual understanding of the problem. Techniques based on the Liapunov stability criterion such as the Popov criteria and circle criteria have been looked into and seem to offer overly restrictive sufficient conditions for stability in most of our reasonably high Q applications. In addition, they fail to extend easily to multiple nonlinear loops.

To facilitate the application of these techniques to the filter conditional stability problem, several interesting results concerning operational amplifiers will first be derived. Earlier nonlinear op-amp models have represented an op-amp by saturating elements intermingled with frequency-dependent networks in a *feedforward* configuration. It will be seen that this is insufficient to predict insertion phase measurements of an op-amp in its nonlinear region. However, the usual position of compensation elements in an op-amp is in a *feedback* path around the gain stages yielding higher effective (Miller effect) capacitances. As a consequence, the linear and nonlinear elements become interconnected in feedback structures which impart varying phase characteristics as a function of amplitude. This becomes highly significant when considering active resonant circuits. Most important, when high Q circuits are realized, any additional phase lag around a loop may be sufficient to increase the pole Q to the point of oscillation. Similar phase shifts may

occur in oscillators in which nonlinearities are purposely introduced to stabilize their amplitude. In oscillators these effects are manifested by a discrepancy between the linearly-computed and actual frequency of oscillation.

Finally, we will present circuits which produce either phase lag or lead as a function of amplitude. These circuits may be useful for nonlinear compensation of the aforementioned problems.

II. THE DESCRIBING FUNCTION TECHNIQUE

The describing function method is an outgrowth of the Harmonic Balance technique used by Krylov and Bogoliubov,[6] in nonlinear mechanics. The method reduces a nonlinear differential equation into a linear relationship by assuming a sinusoidal solution. The method is most useful when the system contains sufficient lowpass filtering to allow higher harmonics to be neglected. However, if the describing function technique is inadequate due to its neglect of higher order harmonics, the DIDF may help in solving the problem.

2.1 *Input-Output Concept of A Nonlinear Element*

We begin our analysis by reviewing some basic concepts of the DF technique. Consider the system of Fig. 1, where the linear and nonlinear parts are assumed separable. N is described in terms of its effect on a sinusoidal waveform. In particular, the describing function is defined as

$$\mathrm{DF} = g(E) \triangleq \frac{\text{Fundamental of } m}{\text{Fundamental of } e} = \frac{M_1}{E} \angle \phi_1 . \tag{1}$$

In general, the DF will be a complex quantity. However, if N is a single-valued nonlinear function, its input-output characteristic will not enclose any area (see Fig. 2) and its DF will always be real as shown in Appendix A.

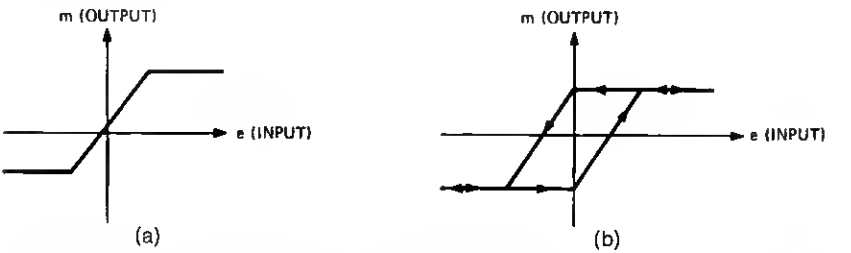

Fig. 2—(a) A single-valued nonlinearity (real DF). (b) A nonlinearity having a hysteresis loop that encloses a given area (complex DF).

On the other hand, the DIDF is defined for a two sine wave input, with one wave at a multiple frequency of the first, i.e.,

$$e = E \cos(\omega t + \phi) + E_1 \cos n\omega t.$$

The DIDF is the ratio of the desired frequency component in the output over the same frequency component at the input. The DIDF has been worked out by West, et al.,[7] for a saturating type of nonlinearity operating on a sinusoidal input in the presence of the third harmonic. This function can be used in determining the required perturbation of the DF when the third harmonic is not sufficiently low for the DF to be directly applicable.

With the above ideas applied to Fig. 1, we may extend linear stability criteria to obtain the stable and unstable limit points for this case. Assuming that there is sufficient lowpass filtering following N in Fig. 1, the input-output relationship of the system is:

$$\frac{v_0}{v_i} = \frac{g(E)H(j\omega)}{1 + g(E)H(j\omega)} \tag{2}$$

$$= \frac{H(j\omega)}{\frac{1}{g(E)} + H(j\omega)}. \tag{3}$$

We now apply the Nyquist criterion, but instead of taking the critical point as -1 and incorporating $g(E)$ into $H(j\omega)$, we take $-[1/g(E)]$ as the critical point.

Figure 3c shows the conventional Nyquist plot and the locus of $-[1/g(E)]$ with E as a parameter for the system the block diagram of which is given in Fig. 3a. The describing function of the nonlinearity,[8] as shown in Fig. 3b depicts the variation in amplitude (the phase shift being zero) of the fundamental of sin ωt operated on by a dead-zone nonlinearity. We note that if E is small, the critical point is not encircled, and the system will be stable. As E is increased, we reach point A, and the system becomes unstable. As a consequence, E increases till we reach point B where the system enters into a stable limit cycle. The limit cycle is stable since if E increases, the system becomes stable causing E to decrease. On the other hand, if E decreases, the system instability is such that E will increase. The intersection point B defines the amplitude (E) and frequency (ω) of oscillation. It is to be noted that in the above case the frequency of oscillation occurs at the intersection of $H(j\omega)$ with the real axis since N introduces no phase shift in this case. However, when N introduces phase shift, this will not be

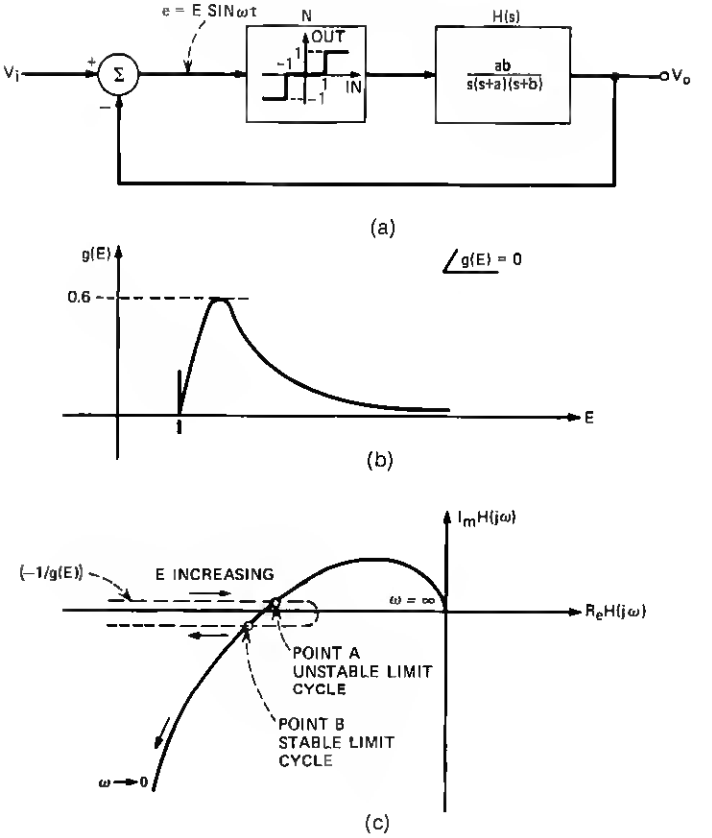

Fig. 3—(a) System with dead-zone relay. (b) DF of dead-zone relay. (c) Nyquist plot.

the case. Furthermore, even when N has a real DF and the second harmonic is not sufficiently filtered out, the DIDF predicts a phase shift of the fundamental through N.

2.2 *Input-Output Concept of A Feedback Structure with Nonlinear Elements in it*

With the above as background, we proceed further with the DF concept by determining the sinusoidal input-output relationship for a feedback system with a nonlinearity. We will do this by considering the specific example of Fig. 4, which resembles an op-amp with unity feedback. As before, we assume sufficient lowpass filtering to eliminate the effect of the second harmonic.

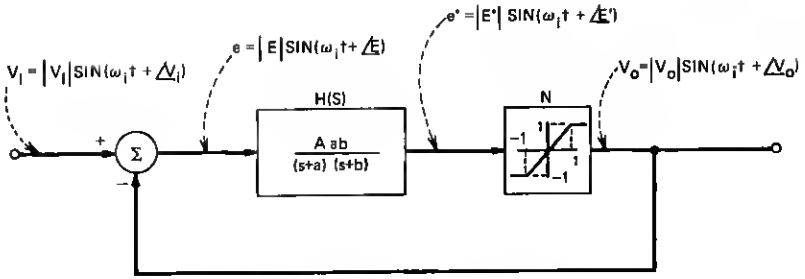

Fig. 4a—System with saturating nonlinearity.

It is clear from Fig. 4a that

$$V_i - V_0 = E \quad \text{or} \quad V_i = E + V_0 . \tag{4}$$

In addition, we know the relationship hetween E and V_0 from the describing function of Fig. 4h and the linear transfer function $H(S)$. Therefore, we can ohtain the relationship hetween V_i and V_0. This is done most appropriately hy considering the phasor diagram of Fig. 5h.

First, we ohtain the transfer characteristics of the linear hlock, $H(j\omega)$ as shown in Fig. 5a. Incidentally, this is the Nyquist plot for the linear region of operation. Assuming momentarily that we hold $\omega = \omega_1$, $H(j\omega)$ and $g(E')$, determine the neccssary magnitudc and phase of E to give a particular V_0. From eq. 4, we then find the corresponding V_i hy taking the vector sum as is shown for several V_0 in Fig. 5h. Ohserve that the houndary hetween the linear and nonlinear region is $(V_0^{(2)}, V_i^{(2)}, E^{(2)})$. In the linear region $\angle V_0 - \angle V_i$ is independent of amplitude, while in the nonlinear region $\angle V_0 - \angle V_i$ is a function of amplitude as shown in Fig. 5c. As a result of $H(j\omega)$, there will he a different curve of this type for each frcquency considered. These curves together with similar ones for $|V_0|/|V_i|$ define the DF for the system

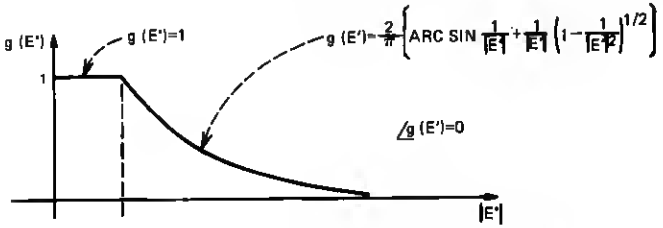

Fig. 4b—Describing function of saturating nonlinearity.

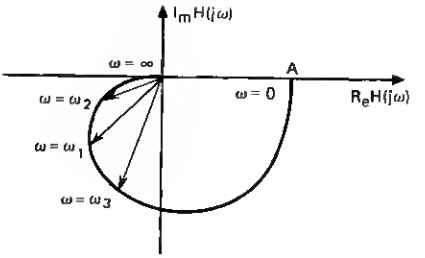

Fig. 5a—Nyquist plot of $H(j\omega)$.

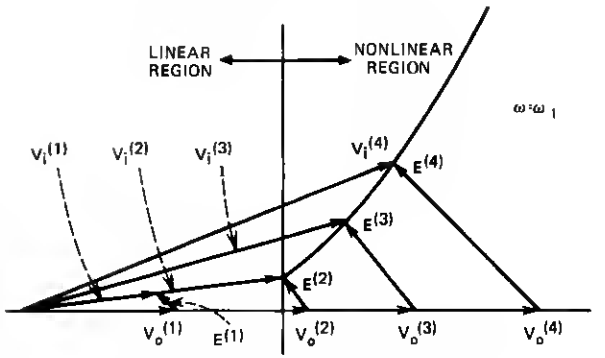

Fig. 5b—Vector diagram for determining V_i.

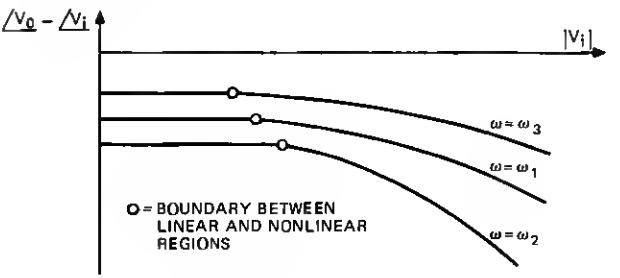

Fig. 5c—Phase shift vs input signal.

of Fig. 4a. This describing function differs slightly from those considered thus far in that it is a function of both amplitude and frequency.

A most important result of the input-output concept developed in this section is the capability of being able to analyze a rather complicated nonlinear network by breaking it up into its constituents. Each one is analyzed individually and then combined as shown in Fig. 6. After

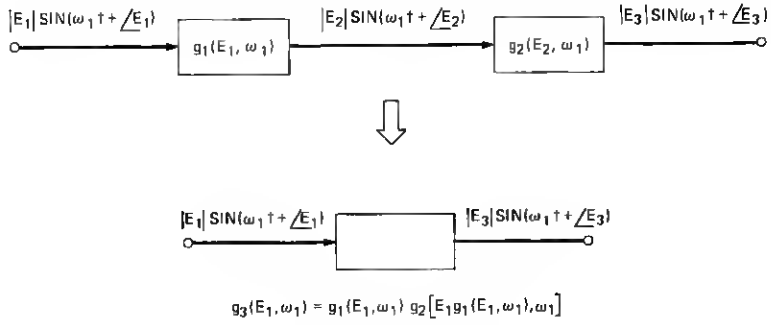

Fig. 6—Interconnection of DF's

reducing the network we apply a variation of the analysis employed for the example of Fig. 3. The difference lies in the fact that the DF is now a function of frequency and amplitude. As a consequence, we ohtain many DF's, each for a particular frequency, of which the negative reciprocal must not intersect the Nyquist plot at that frequency for stahle operation. Usually, as we will see, the critical frequencies correspond to those close to the critical point in the Nyquist plane.

A network which is well suited to this analysis technique is shown in Fig. 7. This is a typical Multiple Amplifier Biquad Filter using monolithic op-amps. Here, it is clear that if we employ the op-amp model shown in Fig. 7h, we have a multifeedhack structure containing several nonlinearities. Deriving the DF of each closed loop op-amp and combining results, we can determine if the phase lag around the loop at certain amplitudes is sufficient to cause the hiquad to oscillate. This is the suhject of the next section.

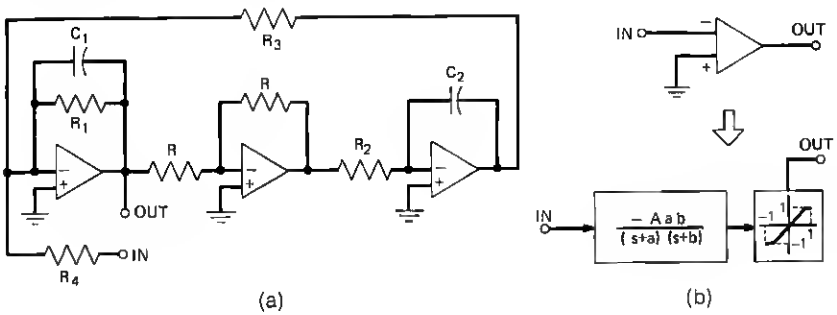

Fig. 7—(a) MAB circuit. (b) A possible model for the op-amp.

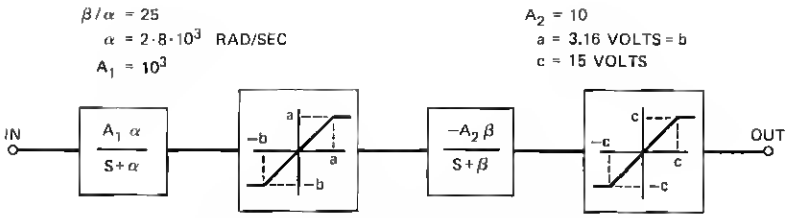

Fig. 8—Fairchild μA709 op-amp model.

III. APPLICATIONS

In this section we shall apply the techniques developed earlier to op-amps, active filters, and oscillators. Since active filters (e.g., MAB and SAB circuits) usually employ monolithic op-amps, we shall develop first an accurate model of the linear and nonlinear aspects of the op-amp. The op-amp model will generally depend on the type (e.g., 709, etc.) and compensation used. However, we shall demonstrate how to arrive at the model and present typical circuits.

3.1 *Operational Amplifiers*

3.1.1 *Open Loop Characteristics of Op-Amps*

We have already presented one possible model of a typical op-amp in Fig. 7h. It is possible to modify the model by placing an amplitude limiter at the input or splitting the linear transfer function by inserting an amplitude limiter. An excellent model, as viewed from pulse and slew-rate measurements on a Fairchild μA 709 op-amp is shown in Fig. 8. The DF for this model does not predict any extra phase shift as a function of amplitude. This follows from Appendix A, where it is shown that this type nonlinearity (no hysteresis) introduces no additional phase shift. However, if we consider the DIDF, we may indeed get extra phase lag as a function of amplitude. This results from the presence of harmonics, generated by the first nonlinearity, at the input of the second nonlinearity. The amount of phase lag may be estimated

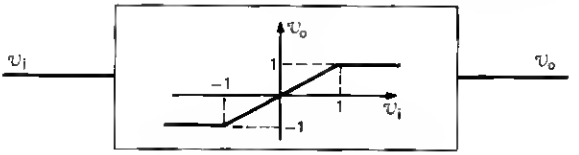

Fig. 9a—Symmetrical saturator.

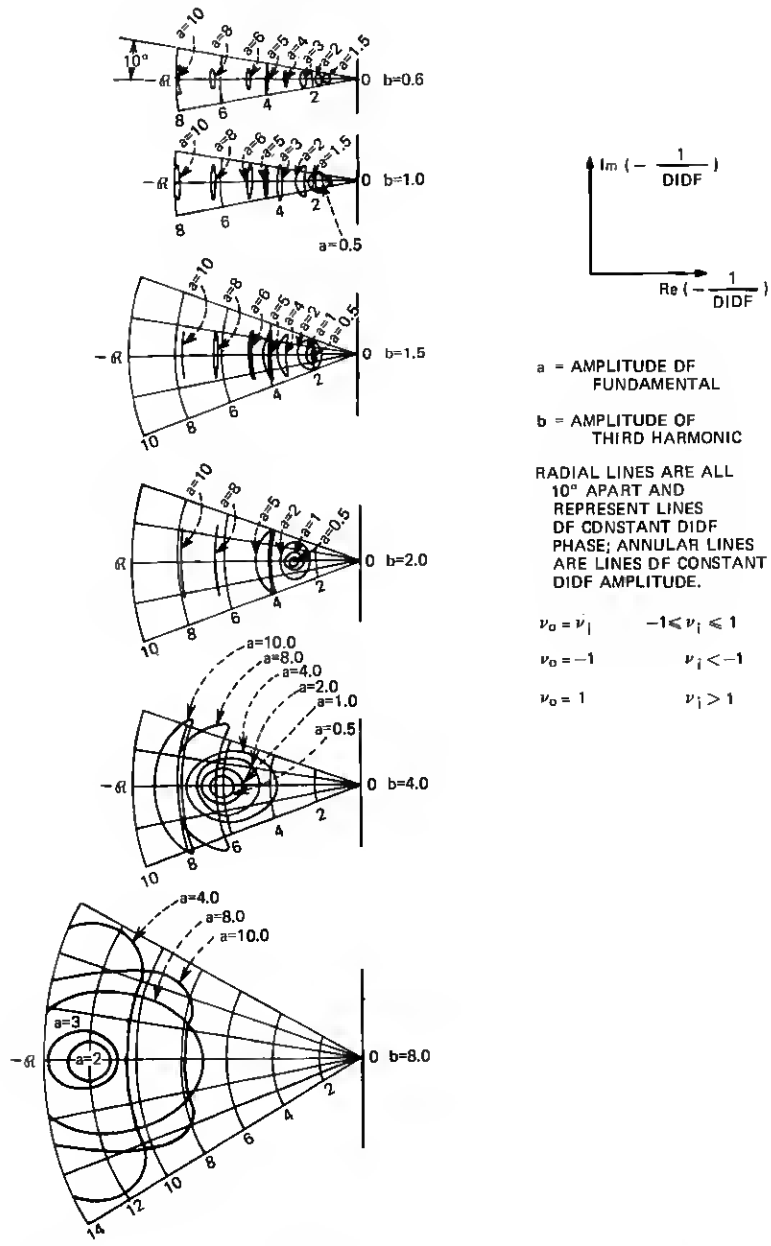

Fig. 9b—Input-output relationships for fundamental in presence of third harmonic for saturating nonlinearity.

hy using the set of DIDF curves for a symmetrieal amplitude limiter[7] shown in Fig. 9. The eurves for each value of a represent the DIDF as a funetion of the phase shift between the fundamental and third harmonic at the input of the saturator.

From these figures, it ean he shown that a maximum fundamental phase lag of 11.1 degrees may he obtained when the op-amp of Fig. 8 is heavily overdriven (i.e., a square wave input to the second saturator). Yet, when the phase eharacteristies of a 709 op-amp were measured in the lab, no sueh effeet was ohserved. The curves ohtained are shown in Fig. 10. These eurves display phase lead as a funetion of amplitude instead of phase lag. This result is extremely important, for it verifies the stability inherent in hiquads at low frequencies as we shall see later. In summary, a hetter model of the op-amp is needed.

To determine this model, we first consider a simple eireuit depieted in Fig. 11. This circuit is a transistorized amplifier whieh provides output limiting of the signal. Its applications include FM limiters and

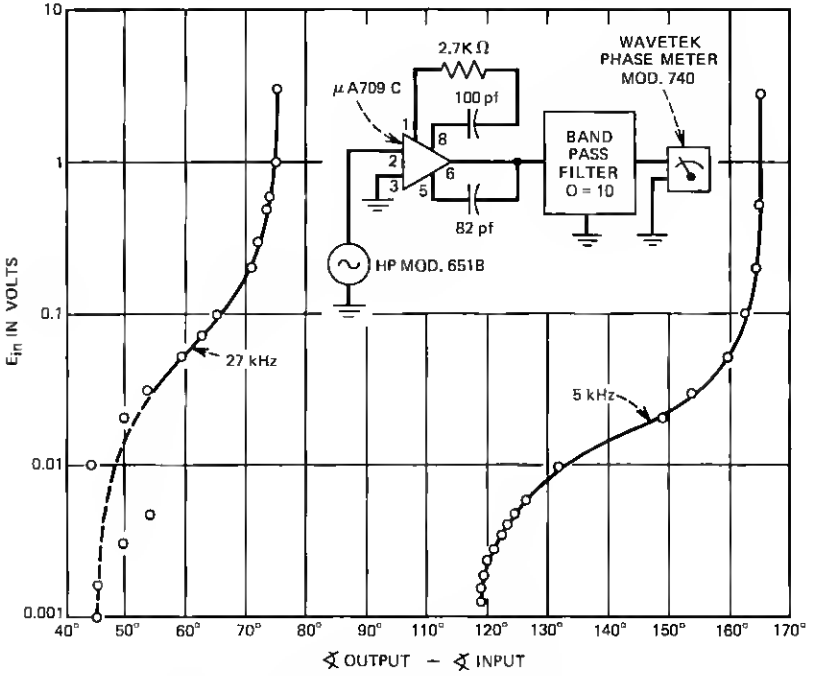

Fig. 10—Measured phase characteristic of an open loop 709 op-amp.

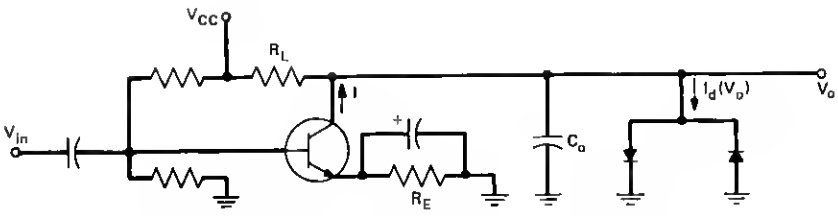

Fig. 11a—Transistor amplifier with output limiting.

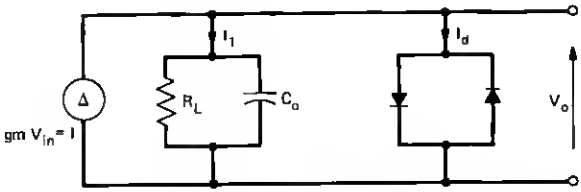

Fig. 11b—Model of Fig. 11a assuming transistor is in linear region.

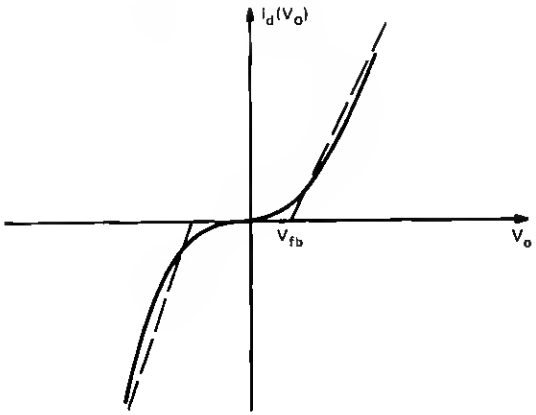

Fig. 11c—Characteristics of diode pair.

amplitude-stabilized oscillators. Defining Z as

$$Z = \frac{R_L}{SC_0R_L + 1} \tag{5}$$

it follows from the circuit that:

$$I = V_0/Z + I_d(V_0) \tag{6}$$

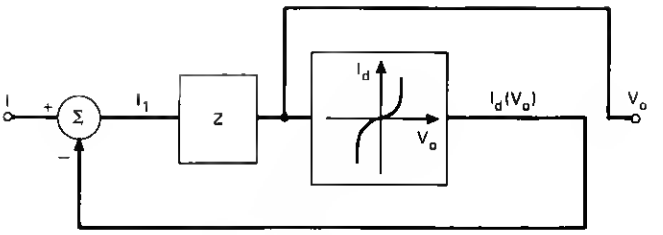

Fig. 12a—Block diagram of Fig. 11b.

or

$$V_0 = Z[I - I_d(V_0)]. \tag{7}$$

This equation is represented by the hlock diagram of Fig. 12a. Knowing the relationship hetween I_1 and I_d, we proceed to draw the phasor diagram of Fig. 12b. Initially at low levels, I_d is small compared to I_1 because thc diodes are cut off. However, if I_1 is just short of turning the diodes on, a slight increase in I_1 will cause a large increase in I_d. These two situations are represented by $(I_d^{(1)}, I_1^{(1)})$ and $(I_d^{(2)}, I_1^{(2)})$ respectively, in Fig. 12b. Taking their vector sum, we ohtain $I^{(1)}$ and $I^{(2)}$. Interestingly we note that the phase difference between I and I_d and hence V_{in} and V_o has decreased. By taking the small signal case as a reference, we conclude that the closed loop network exhibits phase lead with increasing amplitude.

A significant conclusion to be drawn from this example is that although the simple circuit appeared to contain just a clipper (which would indicate no amplitude-dependent phase shift) the feedback present alters the situation sufficiently to predict phase shift as a function of amplitude.

If the same form of analysis is carried out for the internal circuitry

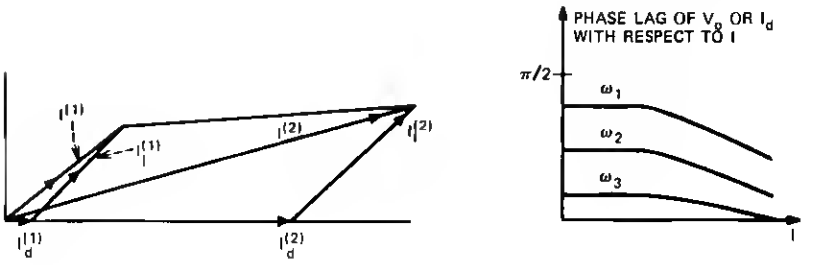

Fig. 12b—Input/output relationship.

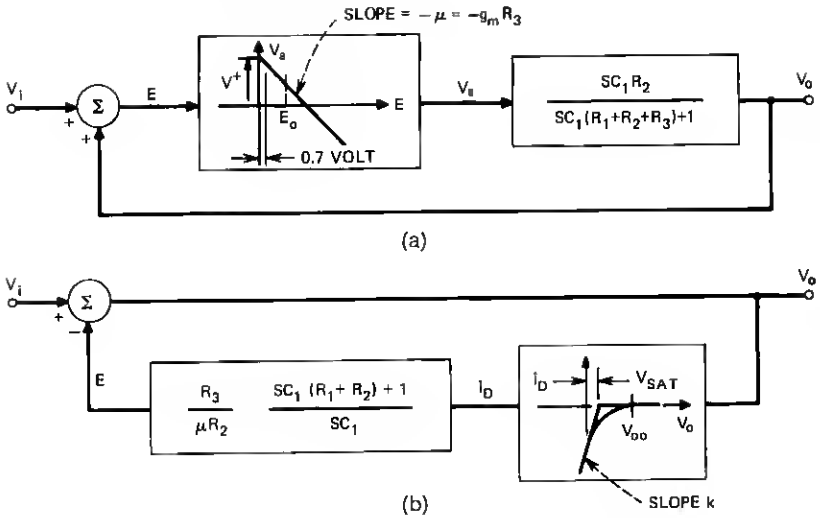

Fig. 13—709 op-amp input compensation circuity model. (a) Cutoff region. (b) Saturation region.

of the 709 op-amp, similar results are obtained. This has been done in Appendix B with particular attention to the circuitry involved in the input and output compensation. Most often, compensation in an op-amp is obtained by making use of the Miller effect to obtain low-frequency breakpoints with relatively small capacitors. Both the input and output compensation in a 709 op-amp take advantage of this effect. As a result, the transistor nonlinearities have RC feedback around them. The equivalent circuits of the input compensation circuitry in the cutoff and saturation regions, as derived in Appendix B, are shown in Fig. 13. In this figure we have left out some linear transfer function blocks at the input and output side, since these have no effect on the

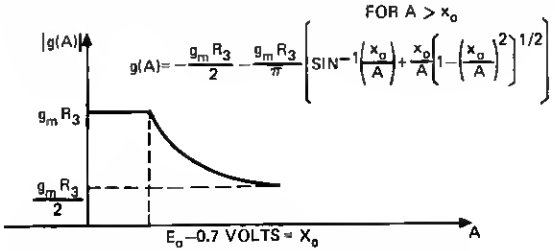

Fig. 14a—DF for nonlinear element in cutoff region model.

nonlinear characteristics. The following analysis will show that both of the circuits in Fig. 13 provide phase lead as amplitude increases.

Figure 14a shows the DF of the nonlinear element[8] in the cutoff region model under the assumption that the quiescent point is at $E = E_0$. Figure 14b depicts the phase relationships of the linear element in that model. With this information and Fig. 13a, we construct the phasor diagram of Fig. 14c. Specifically, since the nonlinear element is single valued and therefore contributes no amplitude sensitive phase shift, $-V_0$ will lead E according to the linear element and the inversion due to the nonlinear element. Entering the nonlinear region of the model, the error voltage E has to increase at a faster rate than V_0 to overcome the attenuation effect of the clipping element. From the relationship

$$V_i = (-V_0) + E \tag{8}$$

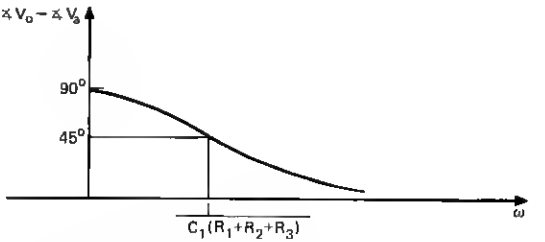

Fig. 14b—Phase characteristic for linear element in cutoff region model.

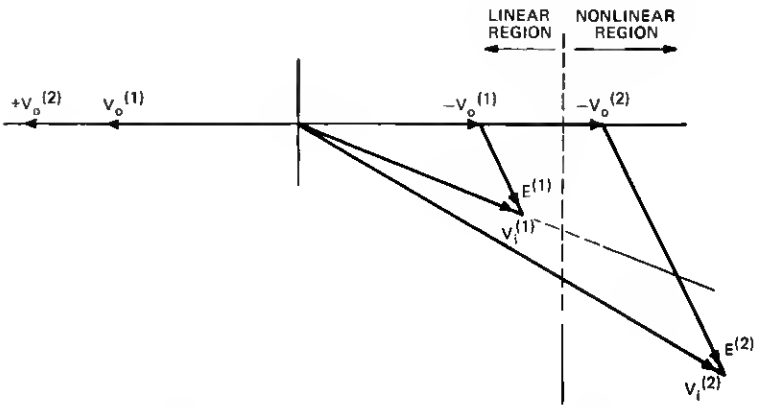

Fig. 14c—Phasor diagram for the closed loop in cutoff region model.

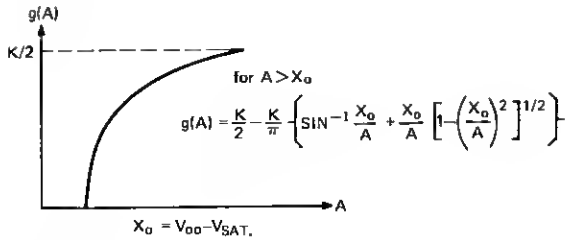

Fig. 14d—DF for nonlinear element in saturation region model.

we determine the third vector V_i. As a result, the angles between $(-V_0^{(1)}, V_i^{(1)})$ and $(-V_0^{(2)}, V_i^{(2)})$ do change with increasing drive. However, at high frequencies where E and $-V_0$ are initially close to being in phase, the increase of phase lead of V_0 relative to V_i is minimal. The frequency breakpoint below which the nonlinear phase lead effect may be expected is typically,

$$f \approx \frac{2}{2\pi(R_1 + R_2 + R_3)C_1} \approx 50 \text{ kHz}. \tag{9}$$

On the other hand, in the saturation region, the model of Fig. 13b applies. Here the DF for the nonlinear element is given in Fig. 14d under the assumption that the quiescent point is at $V_0 = V_{00}$. Furthermore, we have approximated the exponential nonlinearity of the diode in a piece-wise linear manner. It follows directly that the phase relationship of E with respect to V_0 is given by the phase characteristic of the lag network following the nonlinear element in Figure 13. Drawing the phasor relationships for the closed loop at a fixed frequency where the lag network has singificant phase lag yields Fig. 14f. Again, the phasor diagram reveals that the phase lead of V_0 with respect to V_i increases as amplitude increases. The frequencies over which this phase lead

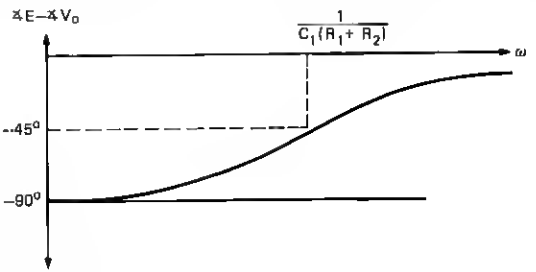

Fig. 14e—Phase characteristics for the linear element in saturation region model.

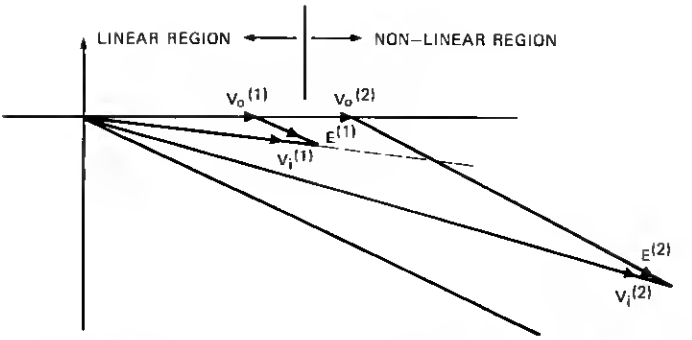

Fig. 14f—Phasor diagram for the closed loop in the saturation region model.

effect will be present is approximately the range of frequencies where the linear network provides phase lag. From Fig. 14e, this occurs for frequencies below:

$$f \approx \frac{2}{2\pi C_1(R_2 + R_1)} \approx 100\,\text{kHz}. \tag{10}$$

Above this frequency range, $E^{(1)}$ and $E^{(2)}$ will have approximately the same orientation as $V_0^{(1)}$ and $V_0^{(2)}$, forcing $V_i^{(1)}$ and $V_i^{(2)}$ to maintain their orientation roughly independent of amplitude.

The above analysis also applies to the output compensation circuitry provided that it is properly interpreted. The output compensation circuitry for a 709 op-amp and its nonlinear model are shown in Fig. 15. Here, unlike the input compensation, the RC network is fed back from an emitter follower circuit which simplifies the model and increases the

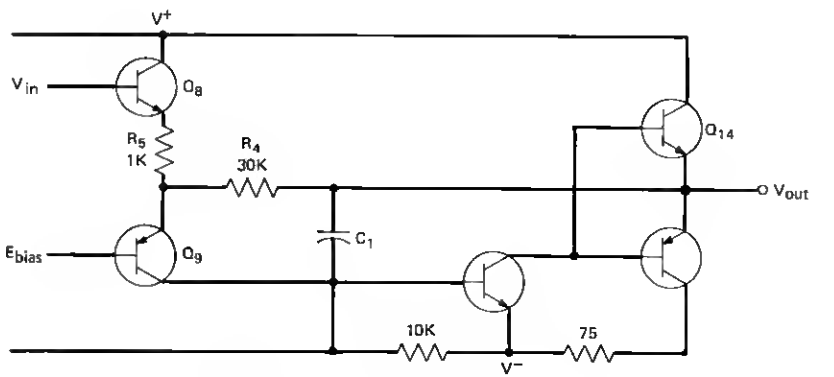

Fig. 15a—Output compensation of 709 op-amp.

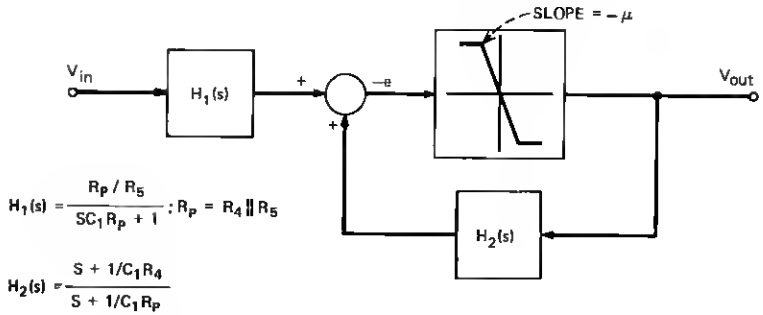

Fig. 15b—Nonlinear model of 709 op-amp.

breakpoint frequencies. In addition, the RC network is fed back to a lower impedance termination which also has the effect of increasing the breakpoint frequencies. In a typical 709 op-amp, this breakpoint frequency occurs at (the equivalent of eq. 9 with R_2 and R_3 being zero)

$$f \approx \frac{1}{2\pi C_1 R_4} \approx 1.5 \times 10^6 \text{ Hz}.$$

This frequency is significantly higher than those resulting from the input compensation (see eqs. 9 and 10). As a result, the output compensation will be quite irrelevant to the conditional stability of biquad filters in the 0 to 100 kHz range. Above 100 kHz, the amplifier will no longer be used in a biquad filter, since the open loop gain is less than 40 dB, which is insufficient for most precision applications.

We now have an op-amp model consistent with the experimental data of Fig. 10. Having discussed these open loop characteristics of an op-amp, we shall next use these concepts to derive the phase properties associated with closed-loop operational amplifiers.

3.1.2 *Closed-Loop Characteristics of Op-Amps*

We shall confine ourselves, in this section, to gain inverters, integrators, and leaky integrators. The circuit of Fig. 16a is the general case which includes all the above-mentioned configurations. The model of the closed loop op-amp shown in Fig. 16c is derived as follows. Assuming that the op-amp has infinite input impedance and letting

$$e_{in} = 0,$$

the voltage developed across the input of the op-amp will be

$$e = \frac{R_1}{R_1 + \left[\frac{1}{SC_1} \| R_a\right]} e_{out} = \frac{SR_1C_1 + R_1/R_a}{SR_1C_1 + [R_1/R_a + 1]} e_{out} . \qquad (11)$$

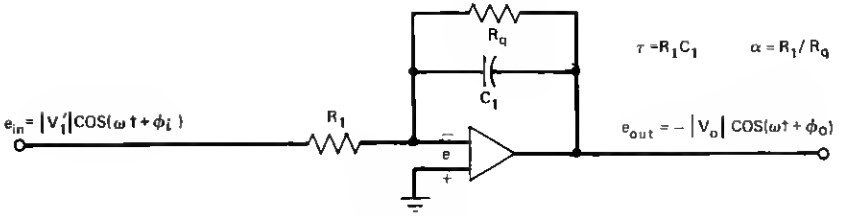

Fig. 16a—Closed loop op-amp.

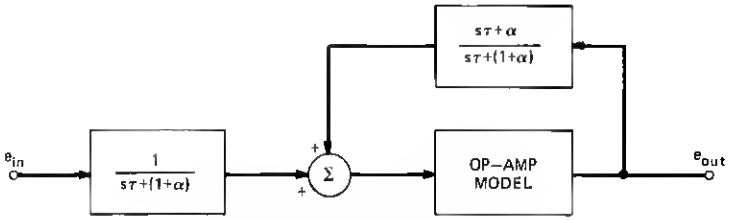

Fig. 16b—Model for Fig. 16a.

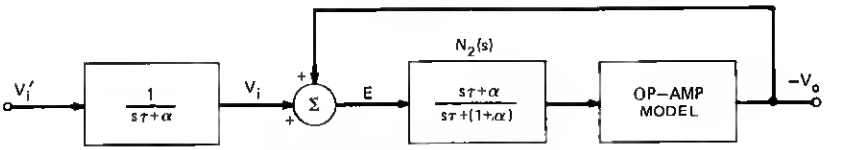

Fig. 16c—Model for Fig. 16a.

Likewise, letting

$$e_{out} = 0,$$

the input voltage of the op-amp will be

$$e = \frac{\frac{1}{SC_1} \,||\, R_q}{R_1 + \left[\frac{1}{SC_1} \,||\, R_q\right]} e_{in} = \frac{1}{SR_1C_1 + [R_1/R_q + 1]} e_{in} . \qquad (12)$$

The block diagram of the closed-loop op-amp, obtained through the superposition of eqs. 11 and 12, is shown in Fig. 16h. By the reduction method, we move the feedback network past the summing node and make the proper correction to the input network. This leaves us with the model of Fig. 16c. A significant advantage of this model is that the ideal transfer function has been separately realized by the network

between V_i' and V_i. Consequently, the feedback network following the ideal transfer function network gives a direct measure of the error introduced by the nonideal characteristics of the op-amp.

For the model of the op-amp itself, we may either use the networks of Fig. 13 in a cascade combination, or we may directly employ the DF curves shown in Fig. 10. The latter method is to be preferred since it is based on actual measurements and requires a minimum of computation. Fig. 17 is the phasor diagram for an inverter (i.e., Fig. 16 with $\tau = 0$ and $\alpha = 1$) at $f = 5$ kHz. In the linear region, we initially obtain a very small error voltage E and consequently V_i and V_0 are almost equal. This error voltage, although small, has a distinct phase lead of approximately 70 degrees with respect to the output voltage V_0. This phase shift is introduced by the frequency characteristics of the op-amp and the network $N_2(s)$ in Fig. 16c. However, for the unity gain inverter, $N_2(j\omega)$ is a real quantity and, therefore, will not add additional phase. As we enter the nonlinear region, the magnitude and phase of the error voltage, E change as dictated by the describing function (DF) of the op-amp. The phase changes according to Fig. 10 and the amplitude according to the real DF of a saturation type of nonlinearity shown in Fig. 4h. Although the op-amp does not behave exactly as a saturation nonlinearity; the magnitude of the DF for the op-amp is well approximated by this DF, unlike the phase shift of the DF which for the saturation nonlinearity is zero.

Having obtained the phasor diagram of Figure 17, we note that increasing the input V_i predicts an increasing phase lag of the output $-V_0$ relative to the input V_i. This effect has been verified experimentally as shown by the curves in Fig. 18. At 27 kHz where the op-amp has

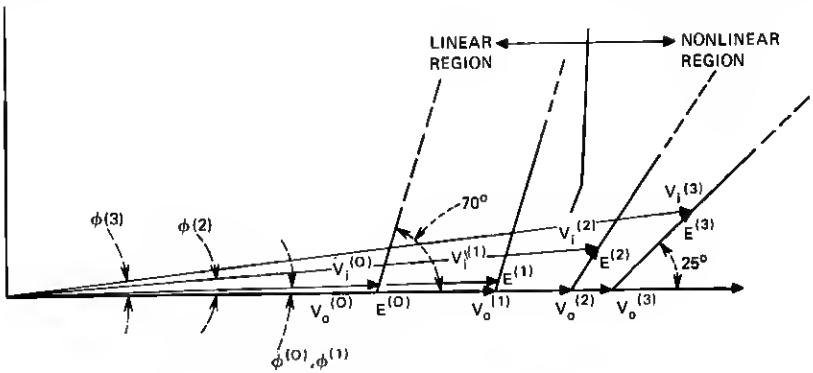

Fig. 17—Phasor diagram for unity gain inverter (using a 709 at 5kHz).

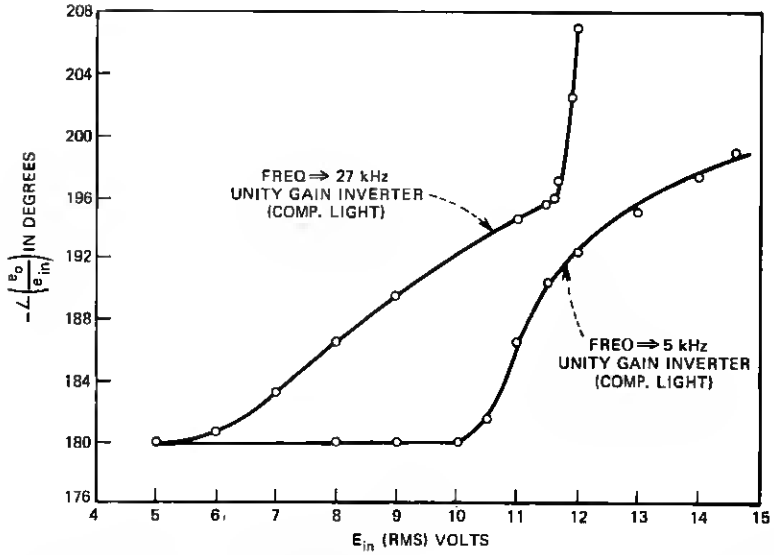

Fig. 18—Measured phase characteristics of a unity gain inverter employing a 709 op-amp.

reduced gain, the effective saturation nonlinearity comes in earlier producing the phase lag at a lower input level.

For the integrator, the same analysis applies but with the critical difference that $N_2(j\omega)$ in Fig. 16c is no longer a real quantity as in the case of the inverter. The phasor diagram for this case is shown in Fig. 19. We have chosen an integrator with $\alpha = 0$ and τ, the reciprocal of angular frequency, $2\pi \cdot 5$ kHz. As a result, $N_2(j\omega)$ will provide a 45-degree lead at 5 kHz, which will have the effect of moving the phase of the error voltage, E, 45 degrees closer to the vector V_0 than in the

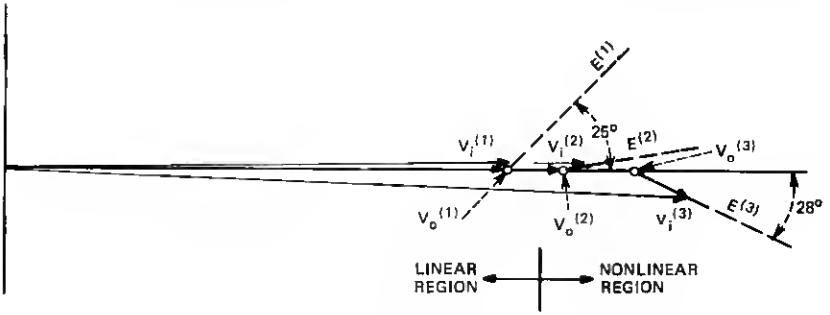

Fig. 19—Phasor diagram for integrator at 5kHz, $\tau = 1/2\pi 5$kHz, $\alpha = 0$.

case of the inverter. However, when the system is overdriven, E swings around to the lagging side of V_0, which consequently causes V_0 to lead V_i. As a result, in the integrator at this frequency, increasing the drive level produces a phase lead effect. This has been verified experimentally and the results are shown in Fig. 20.

3.2 *Active Filters*

3.2.1 *The Multiple Amplifier Biquad Filter*

The above discussion has provided a basic feel for what happens when the op-amp is employed in a simple feedback loop. We shall next discuss the performance of networks which use these inverters or integrators as building blocks.

The MAB[2] circuit was already shown in Fig. 7a in its bandpass configuration. The configuration generates a pair of poles with arbitrary Q and frequency location. To generate a pair of zeroes, outputs taken at different points are summed in a separate summing amplifier. The zeroes can also be generated by feeding the input to more than one op-amp as is done in the Multiple Input Biquad Filter (MIB). However, their basic operational frequency limitation manifests itself by a conditional stability problem in its pole forming loop. This problem is more acute when high Q's are desired, for then the resonator loop operates very close to the critical point of its Nyquist plot. This is shown in Fig. 21, where it is seen that the phase shift around the loop at the pole frequency gets very close to 180 degrees as the Q is increased.

As a consequence, a small amount of additional phase lag in any of the amplifier blocks (i.e., the inverter and the leaky and nonleaky integrators) making up the main loop can make the system unstable.

With the information already acquired, as to the characteristics of

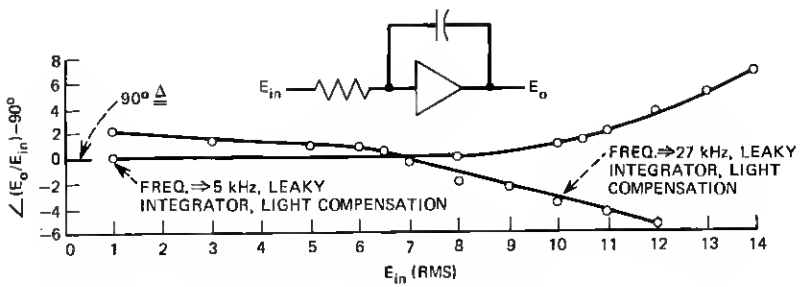

Fig. 20—Measured phase characteristics for integrator employing a 709 op-amp (the gain is unity).

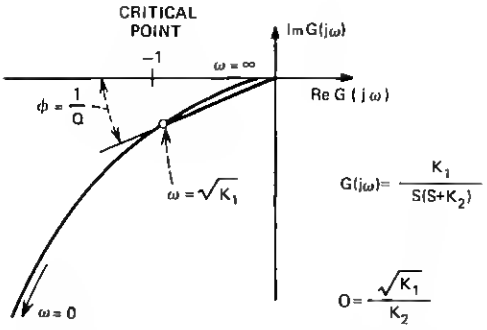

Fig. 21—Nyquist plot for main loop in MAB.

the individual amplifier blocks, the task of determining whether a given filter will be stable can be investigated. By adding up the phase shift curves of the individual amplifiers, as determined from Figs. 18 and 20, we are able to determine if the outer loop is stable with increasing drive level. As an example, we shall consider a MAB circuit which has a pole frequency at 5 kHz with a Q of 20. The design is such that

$$\omega = \frac{1}{\sqrt{R_3R_2C_1C_2}} = \frac{1}{R_3C_1} = \frac{1}{R_2C_2} = 2\pi \cdot 5 \cdot 10^3$$

and

$$Q = \frac{R_1}{R_3} = 20.$$

In this case, the integrators will have approximately unity gain at the resonant frequency of the pole. Consequently, all the three amplifiers enter the nonlinear region at roughly the same level. From the given Q we determine the phase lag needed to bring the main loop into oscillation at the pole frequency. For the reasonably high Q of 20, this is given by:

$$\phi_n = \frac{1}{Q} = 0.05 \text{ rad} \cong 2.9°.$$

Referring back to the phase characteristics of the inverter in Fig. 18, we note that in the inverter, phase lag is introduced as the input level is increased. However, this is counterbalanced by the phase lead introduced by the integrator (see Fig. 20).

It is to be noted that for very high input levels where the phase lag of the inverter becomes dominant, the circuit will, nevertheless, be stable. This results from the sharp drop in the magnitude of the DF

when the amplifiers are heavily saturated. The drop in the magnitude of the DF has the effect of shifting the critical point toward the left in the Nyquist plot of Fig. 21.

If the same circuit is scaled up to 27 kHz, the outer loop will undoubtedly be conditionally stable. In this case, both the inverter and integrator provide phase lag (Figs. 18 and 20) and at the level which produces 2.9-degree phase lag, the circuit will become unstable. As the signal level increases, due to the instability, the circuit will reach a stable limit cycle where the magnitude of the DF has decreased sufficiently to just touch the Nyquist curve.

The method of analysis employed thus far has its greatest advantage in that it is able to suggest many ways of getting around the stability problem in MAB filters. These methods center in either improving the manner in which the magnitude of the DF drops (possibly by making this occur earlier so that it becomes dominant) or improving the phase characteristics of the DF. One method which has been employed successfully is the use of a diode network across the leaky integrator. This has the effect of improving both of the DF characteristics, magnitude and phase. This circuit and the model for it are shown in Fig. 22. The model in Fig. 22c is derived very simply by taking

$$i = i' \text{ and } 0 \text{ volt at op-amp input.}$$

We then have,

$$i = \frac{-e_{in}}{R_1} = i_d(e_0) + e_0 SC_1 + \frac{e_0}{R_Q} = i'$$

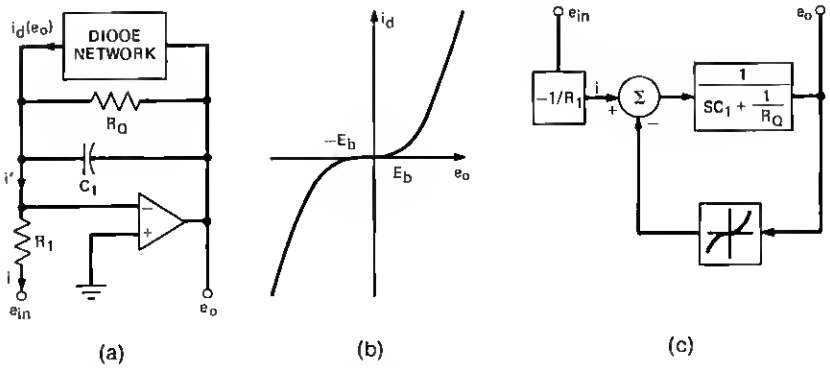

Fig. 22—(a) Diode network across integrator. (b) I/O characteristics of the diode network. (c) Model for (a).

which if rearranged, we get the equation describing the model

$$e_0 = \left[\frac{-e_{in}}{R_1} - i_d(e_0)\right] \frac{1}{SC_1 + \frac{1}{R_Q}}.$$

Drawing a phasor diagram for this circuit reveals that the magnitude of the DF drops and simultaneously phase lead is introduced as signal level increases. It is worthwhile to point out that limiting directly at the output of the op-amp has the opposite effect (as shown earlier in the example of Fig. 4); therefore, limiting cannot be blindly applied. This technique has been employed in a MAB using 709's to obtain a Q of 50 at 100 kHz. Above this frequency, the gain of a 709 op-amp is no longer sufficient to give a precision filter. Similarly, a MAB employing 702 op-amps was made to operate at 2 MHz with a Q of 10.

This method of nonlinear compensation has the disadvantage of limiting the dynamic range of the filter. Therefore, techniques which compensate the op-amps internally are more desirable. It has been shown in Section II how internal compensation affects the DF of closed loop amplifiers. In turn, these circuits may be rearranged to produce better characteristics. We will not dwell on this subject in great detail; however, we shall discuss the connection with slew rate. It is well known that slew rate limiting in operational amplifiers is caused by some form of either voltage or current limiting. Consequently, as a result of this limiting, we may expect that the DF and, therefore, conditional stability will be affected. However, this may not necessarily be the case for it may happen that the limiting element causing slew rate is not the dominant factor in determining the phase characteristic of the op-amp. This is most vividly illustrated by a 709 op-amp with input and output compensation. It has been experimentally observed that the input compensation affects the frequency range of conditional stability while the output compensation has a negligible effect. On the other hand, slew rate limiting is mostly affected by the output compensation. The dominance of the input compensation in controlling conditional stability is consistent with our derivation of the DF of an open loop 709 op-amp.[9]

3.2.2 *The Single Amplifier Biquad Filter*

The single amplifier biquad[1] circuit is shown in Fig. 23a. In Figs. 23b and c, we have the feedback structure, as seen by the op-amp, and its Nyquist plot. Here, once again, we deal with a single op-amp in a closed loop configuration and our interest lies in determining its stability.

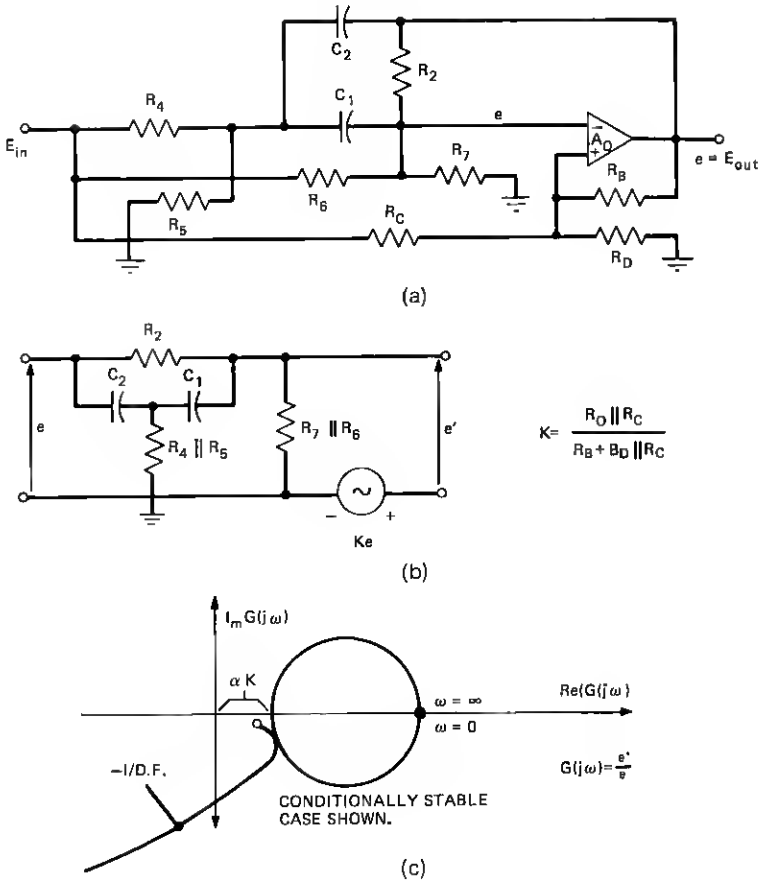

Fig. 23—(a) SAB Circuit. (b) Feedback structure as seen by op-amp. (c) Nyquist plot of feedback structure assuming $R_7 \| R_6 \gg R_2$.

From the open loop DF curves of the op-amp, we can plot the locus of the critical points as $-1/DF$. As shown in Fig. 23c, the circuit is conditionally stable as a result of more than 90 degrees of phase lag in the amplifier. One manner in which stability can be achieved is by appropriately including a diode network in the feedback structure such as to move the circle in Fig. 23c to the right when the drive level exceeds a predetermined threshold. This network can either be placed across R_2 or R_D. Another alternative, which is advantageous from a dynamic-range perspective, is to design the op-amp or its compensation such

that proper phase lead is introduced sharply as the level is increased. Modified forms of the compensation circuitry discussed in Section 3.1 can be used to achieve this effect.

3.3 *Amplitude Stabilized Oscillators*

Sine wave oscillators are usually designed in the linear domain by placing the poles slightly to the right of the $j\omega$-axis in the S-plane. If the network remained in its linear region, the network output would increase exponentially without bound. Invariably, therefore, nonlinearities are introduced to produce a stable limit cycle. Fig. 24 illustrates a typical circuit which makes use of a saturation type of nonlinearity. Since the DF of a saturating nonlinearity is real, the circuit will oscillate at the frequency of the tuned circuit, independent of the nonlinearity.

Many times, especially at high frequencies, nonlinearities with an effective real DF are difficult to obtain. In these cases, the computation of the DF (as a function of amplitude and frequency) is required to determine both the amplitude and frequency of the limit cycle. To illustrate this point, we refer to the oscillator of Fig. 25. (This circuit is being currently employed in a 20-MHz subcable oscillator. In this application, reliability necessitates an accurate determination of the frequency of oscillation.) A first look at the circuit may lead us to the conclusion that it behaves in the same manner as the oscillator shown in Fig. 24a. The pair of diodes would behave as the saturating nonlinearity while the frequency selectivity would be provided by the tank circuit. However, a second look reveals that this circuit is quite similar to that shown in Fig. 11. It can also be seen, recalling Fig. 12,

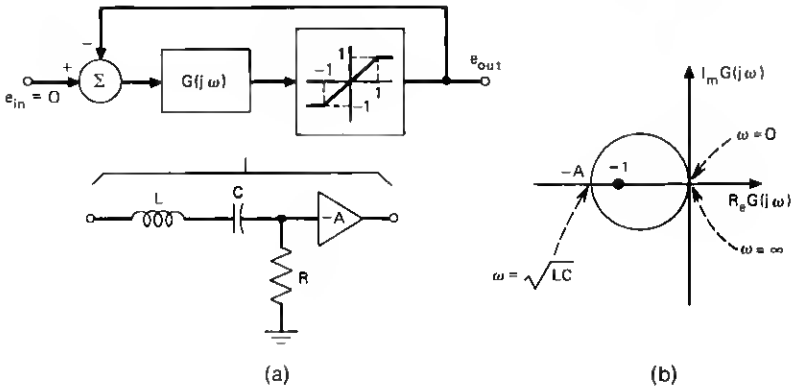

Fig. 24—(a) Amplitude-stabilized oscillator. (b) Nyquist plot.

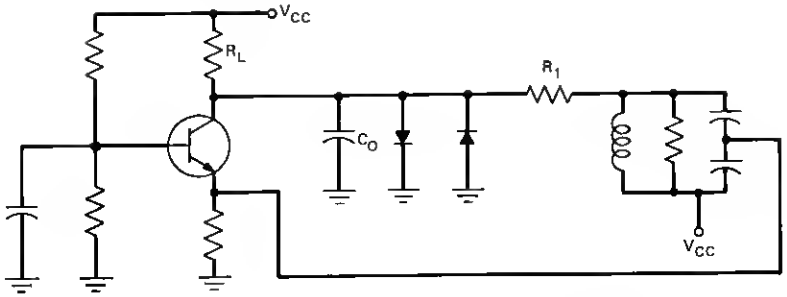

Fig. 25—Amplitude-stabilized oscillator by the use of diodes.

that the pair of diodes is effectively in a feedback configuration with frequency-sensitive elements, which produces a complex DF. Therefore, we conclude that this circuit will have an oscillation frequency dependent on the nonlinearity.

IV. CONCLUSION

A technique which analyzes the stability of frequency-selective feedback structures containing nonlinearities has been presented. This technique is an adaptation of the describing function technique to include multiple feedback structures. This is accomplished by extending the definition of the conventional describing function to include networks containing nonlinearities around frequency-dependent linear elements. By doing so, the describing function of typical operational amplifiers in open and closed loop configurations have been derived. These, then, serve as a means of predicting the conditional stability criteria in frequency-selective feedback networks such as the Multiple Amplifier Biquad and the Single Amplifier Biquad. A valuable result of this analysis is the discovery of circuits which circumvent in one way or another the conditional stability of high-frequency biquads. This result has had a highly beneficial impact on high-frequency biquads since it relieves the conditional stability problem and shifts emphasis to the maximum open-loop gain available at high frequencies. This open-loop gain determines the precision which high Q circuits can achieve at these high frequencies.

V. ACKNOWLEDGMENTS

Many of the techniques described in the memorandum came about through the special efforts of R. L. Ukeiley. He has spent long hours

in gathering important data relating to the maximum operating frequencies for MAB's and open and closed loop op-amp measurements. As a matter of fact, it was he who first observed the lack of correlation between slew rate and conditional stability. I am also indebted to J. J. Friend for his many suggestions and to R. C. Drechsler for his patient efforts in guiding this project.

APPENDIX A

A Property of the Imaginary Part of A Describing Function

Theorem: The imaginary part of the describing function, $G(A)$, associated with a multiple valued input-output function, $f(a)$, is given by

$$\text{Im } \{G(A)\} = \frac{-S_A}{\pi A^2}$$

where $S_A \triangleq$ area enclosed by $f(a)$ for $|a| < A$; positive when path taken by nonlinearity is in a counterclockwise direction.

Proof:

$$\text{Im } \{G(A)\} = \frac{1}{A\pi} \int_0^{2\pi} f(A \sin \omega t) \cos \omega t \, d(\omega t). \tag{13}$$

Let,

$$\mu = A \sin \omega t.$$

Then,

$$d\mu = A \cos \omega t \, d(\omega t).$$

It follows by substitution into eq. 13 that,

$$\text{Im } \{G(A)\} = \frac{1}{A^2\pi} \oint_{|\mu|<A} f(\mu) \, d\mu = -\frac{S_A}{\pi A^2} \qquad \text{Q.E.D.}$$

APPENDIX B

709 Op-Amp Models

The schematic of the input circuitry of a μ709 op-amp is shown in Fig. 26. The transistors Q_4 and Q_6 make up the second stage of amplification. Q_3, Q_5, and Q_7 decode the differential output of Q_1 and Q_2 providing a single-ended signal at the base of Q_4. The input compensation, a series RC network, is placed across base and collector of the Darlington pair, Q_4 and Q_6. This provides (together with the

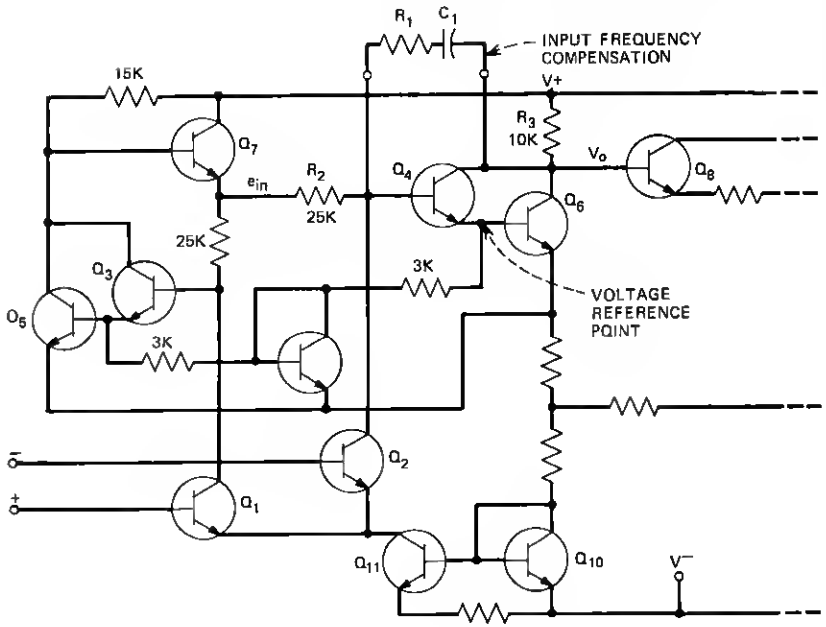

Fig. 26—Input circuitry of μA 709 op-amp.[10]

output compensation) the necessary frequency rolloff to stabilize the amplifier in the linear domain.

Fig. 27 depicts the approximate circuit model of the second-stage amplifier derived from the Ebers–Moll model.[11] We have assumed that the input impedance of the Darlington stage is much larger than R_2 and the load impedance presented by the emitter follower, Q_8, is negligible compared to R_3. The cutoff region is represented by the characteristics of V_a, shown in Fig. 27b. Saturation is introduced in the model by the diode D. In Fig. 27a the current I is given by

$$I = \frac{e_{in} - V_0}{R_2 + R_1 + \dfrac{1}{SC_1}} = \frac{V_0 - V_a(V_{be})}{R_3} + i_D(V_0)$$

Rewriting this equation, gives

$$V_0 = \frac{Z_2}{Z_1} e_{in} + V_a(V_{be}) \frac{Z_2}{R_3} - i_D(V_0) Z_2 \tag{14}$$

where,

$$Z_1 \triangleq R_1 + R_2 + \frac{1}{SC_1}$$

$$Z_2 = \frac{Z_1 R_3}{Z_1 + R_3}.$$

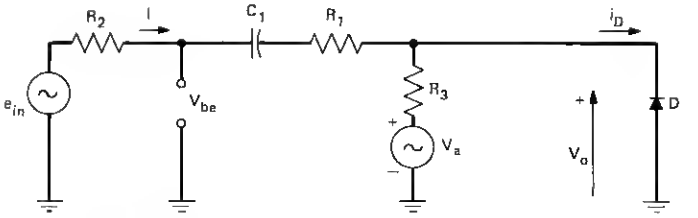

Fig. 27a—Circuit model for the second-stage amplifier.

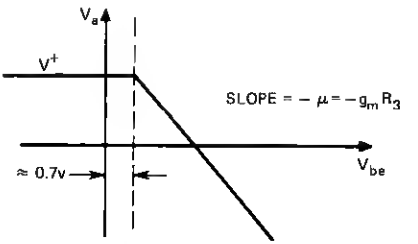

Fig. 27b—Nonlinear elements of the second stage amplifier corresponding to the cutoff region.

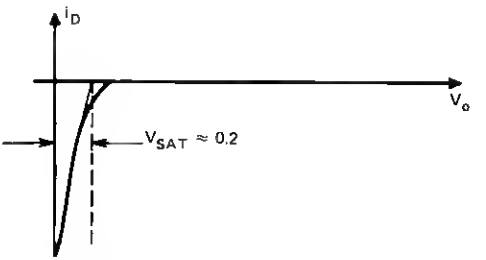

Fig. 27c—Nonlinear elements of the second stage amplifier corresponding to the saturation region.

We also obtain from Fig. 27a

$$V_{be} = e_{in} - \left(\frac{e_{in} - V_0}{Z_1}\right)R_2$$

$$= e_{in}\frac{R_2}{Z_3} + V_0\frac{R_2}{Z_1} \tag{15}$$

where,

$$Z_3 = \frac{Z_1 R_2}{Z_1 - R_2}.$$

Figure 28 is a block-diagram representation of eqs. 14 and 15. For simplicity, we distinguish between the cutoff and saturation regions. The result of this is shown in Fig. 29. In both models, the forward path containing Z_2/Z_1 in Fig. 28 is neglected since the other path through V_a has a much larger gain. We have also assumed, with some loss of generality, that the biasing is such that a sufficiently high drive level producing cutoff (saturation) does not cause saturation (cutoff) during some other portion of the cycle. However, in general, the problem can be solved by computing the DF for the inner loops involving i_D and V_a and employing these results to solve for the DF for the complete system.

The model of Fig. 29a represents the second-stage amplifier when driven into cutoff. It is obtained directly from Fig. 28 by making a slight rearrangement at the output in addition to the two previously

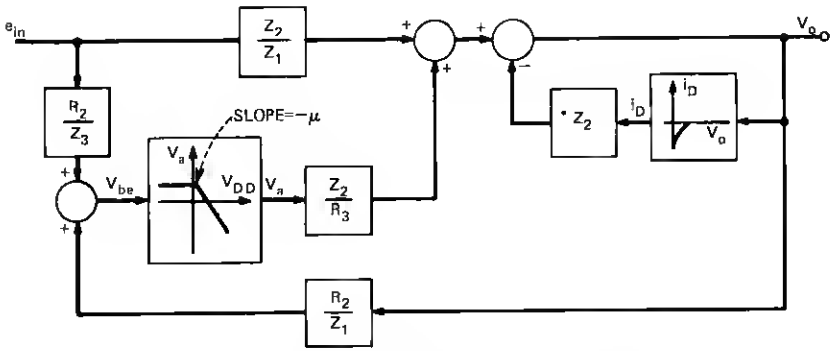

Fig. 28—Block diagram representation of eqs. 14 and 15.

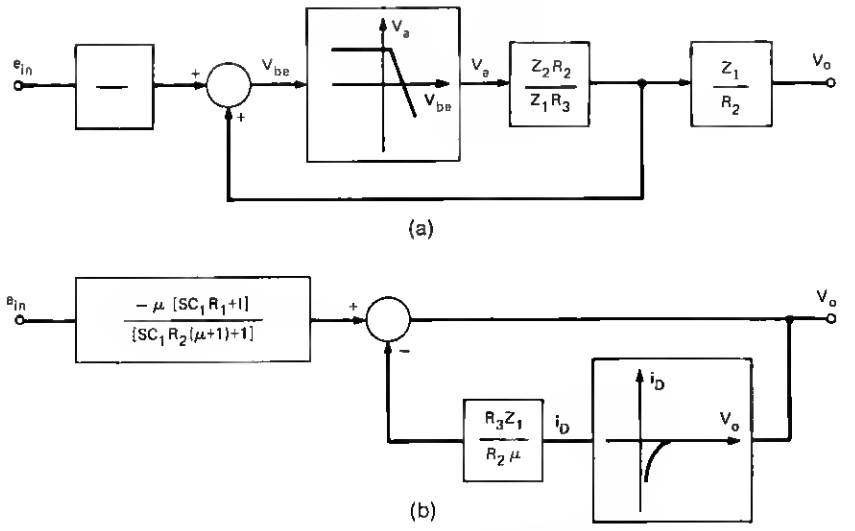

Fig. 29—(a) Model for the cutoff region. (b) Model for the saturation region.

mentioned assumptions. The network parameters are given by

$$\frac{Z_2R_2}{Z_1R_3} = \frac{SC_1R_2}{SC_1(R_1 + R_2 + R_3) + 1}$$

$$\frac{R_2}{Z_3} = \frac{SC_1R_1 + 1}{SC_1(R_1 + R_2) + 1}$$

$$\frac{Z_1}{R_2} = \frac{SC_1(R_1 + R_2) + 1}{SC_1R_2}.$$

The model shown in Fig. 29a depicts the saturation region. It is obtained from Fig. 28 by restricting V_a vs V_{be} to operate in the linear region. Consequently, this nonlinear element (V_a vs V_{be}) in Fig. 28 becomes a linear gain element. The process of reduction is shown in Fig. 30. Figure 30c, after factoring out the feed-forward path and assuming a large μ, yields the saturation model of Fig. 29b. The linear element in the feedback loop in terms of fundamental parameters is:

$$\frac{R_3Z_1}{R_2\mu} = \frac{R_3}{R_2\mu}\left[\frac{SC_1(R_1 + R_2) + 1}{SC_1}\right].$$

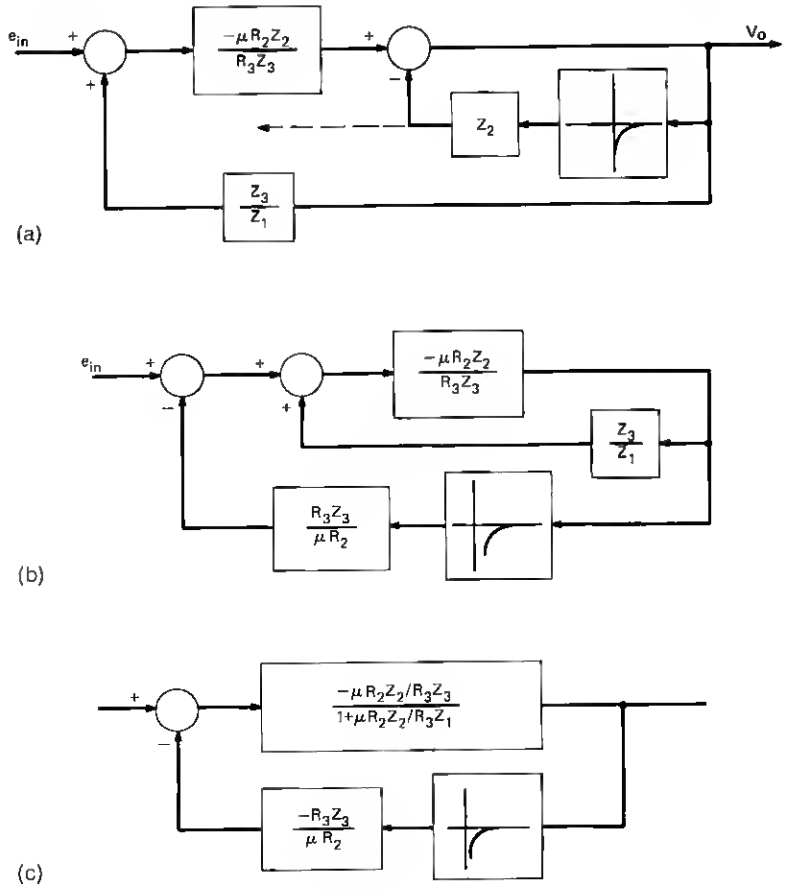

Fig. 30—Reduction of Fig. 28.

REFERENCES

1. Friend, J. J., "A Single Operational Amplifier Biquadratic Filter Section," 1970 IEEE International Symposium on Circuit Theory Digest, December 14–16, 1970, pp. 179–180.
2. Thomas, Lee C., "The Biquad: Part I—Some Practical Design Considerations" and "The Biquad: Part II—A Multipurpose Active Filtering System," IEEE Trans. Circuit Theory, *CT-18* (May 1971), pp. 350–361.
3. Goldfarb, L. C., "On Some Nonlinear Phenomena in Regulatory Systems," Automatika i Telemekanika, *8*, No. 5 (September–October 1947), pp. 349–383.
4. Gibson, J. E., *Nonlinear Automatic Control*, New York: McGraw-Hill, 1963, pp. 203–235, 343–438.
5. Siljak, D., *Nonlinear Systems*, New York: John Wiley, 1969, Chapters 3, 4, 5, 6, 7 and App. F and G.

6. Krylov, N., and Bogoliubov, N., *New Methods in Nonlinear Mechanics*, Moscow: State Publishing House, 1934.
7. West, J. C., Douce, J. L., and Livesly, R. K., "The Dual Input Describing Function and Its Use in the Analysis of Nonlinear Feedback Systems," Proc. IEEE, *103*, Part B, 1956, pp. 463–474.
8. Op. Cit., Siljak, D., pp. 472, 481, 498–510.
9. Ukeiley, R. L., private communication relating to unpublished data concerning frequency and slew rate limitations.
10. Giles, J. N., *Fairchild Semiconductor IC Applications Handbook*, Fairchild Semiconductor, 1967, pp. 57–59.
11. Angelo, Jr., E. J., *Electronics: BJT's FET's and Microcircuits*, New York: McGraw-Hill, 1969, pp. 245–250.